PERGAMON

International Journal of Heat and Mass Transfer 44 (2001) 1947–1962

International Journal of HEAT and MASS TRANSFER

www.elsevier.com/locate/ijhmt

Flow and heat transfer regimes in inclined differentially heated cavities

R. Delgado-Buscalioni *, E. Crespo del Arco

Departamento de Física Fundamental, Universidad de Educación a Distancia, Senda del Rey s/n, E-28040 Madrid, Spain

Received 18 October 1999; received in revised form 30 June 2000

Abstract

The natural convection in long inclined cavities with differentially heated end walls is analytically and numerically studied. The dimensionless axial temperature gradient at the core region, K, is calculated and it is used to determine the frontiers of the flow regimes (conductive, transition and boundary layer regimes) in the space of parameters. For horizontal cavities ($\alpha = 90°$) these frontiers have been found at $A^2Ra \simeq 10^2$ and $A^2Ra \simeq 10^4$, and confirm the results of B. Boehrer (Convection in a long cavity with differentially heated end walls, Int. J. Heat Mass Transfer 40 (17) (1997) 4105–4114). For $0 < \alpha < 90°$ (heated-from-below cavities) the frontiers are found at values of the group parameter $ARa\cos(\alpha)/R_0$ of order 1 and 10. If the cavity is heated from above the flow always remains in the conductive regime if α is made large enough (typically $\alpha > 100°$). The boundary layer regime (BLR) for $\alpha < 90°$ is also studied. If the cavity is inclined, no stagnant region is formed at the center of the core, but instead a region with approximately constant shear. In the BLR, the maximum cross-stream and axial velocities scale, respectively, with $Ra^{1/4}$ and $Ra^{4/7}$ and the transport of heat in the core, governed by the axial advection, grows like $Nu \sim Ra^{2/7}$. Numerical calculations of the flow in a closed geometry carried out by a Chebyshev-collocation method confirm the theoretical predictions and are used to investigate the structure of the flow at large Rayleigh number.

1. Introduction

The study of natural convection in shallow inclined cavities driven by end-to-end temperature difference is applied in different domains of industry and nature. For instance, in crystal growth processes from melts, larger transport rates are obtained by tilting the ampoule [2]. This fact has motivated some experimental and numerical simulations of the hydrodynamic aspects of crystal growth processes in tilted ampoules with axial heating [3]. Also in heat exchangers it has been proved that the heat transfer is enhanced when the tube is optimally inclined [4]. Another application of the inclined configuration is to honeycomb solar collector plates, where the low aspect ratio enclosure may be thought of as a single cell of the honeycomb structure [5,6]. The study of natural convection in tilted shallow fluid layers is also relevant in many geophysical situations where the fluid is enclosed in long narrow slots arbitrarily inclined to gravity [7,8]. A particular important example of application in this field is the study of the transport rate of spread of passive contaminants such as radioactive materials in long tilted liquid filled rock fractures [7]. Concerning fundamental research, the inclined configuration is a simple system which allows the study of several types of instabilities and their corresponding interactions by making a suitable choice of the values of the external parameters. This was revealed by theoretical and numerical studies on the stability of the base flow in this particular configuration [9]. Also recent experiments on natural convection in cavities with axial and lateral heating have used tilted geometries to study the interaction between longitudinal and transversal instabilities [10]. The stability thresholds depend on the local Rayleigh number at the core region and to correctly predict the onset of the instabilities it is necessary to know the value of the axial temperature gradient at the core.

In the extensive literature on horizontal cavities (see [1] for a chronological review of the problem), the

* Corresponding author.

0017-9310/01/$ - see front matter
PII: S0017-9310(00)00242-8

Notation

A	aspect ratio, H/L
F	function associated to the heat flux advected from the core, Eq. (15)
g	gravity acceleration
H	width of the cavity (x-direction)
K	dimensionless axial temperature gradient at the core
L	length of the cavity (z-direction)
Nu	Nusselt number
$Nu_{\mathscr{R}}$	reduced Nusselt number, Eq. (35)
M_w, M_t	functions for the dependence on α of respectively, $W_{\max}$ and Θ_x
r	core flow profile parameter
Pr	Prandtl number, ν/κ
r_0	lowest non-trivial solution of $\tan(r)+\tanh(r)=0, r_0 \simeq 2.365$
R_0	critical Rayleigh number for convection in an infinite vertical cavity, $2r_0^4$
Ra	Rayleigh number, $g\beta\Delta T H^3/\nu\kappa$
T	dimensionless temperature
ΔT	dimensional temperature difference between the end walls
$\mathscr{R}$	group parameter, $ARa\cos(\alpha)/R_0$
$\boldsymbol{v}=(u,w)$	dimensionless velocity (along x- and z-direction)
$U_{\max}, W_{\max}$	maximum dimensional velocities along x- and z-directions
x, z	coordinates along cross-stream and axial directions, respectively.

Greek symbols

α	inclination respect vertical position, [°]
β	coefficient of thermal expansion
δ	match parameter in the Bejan and Tien's model
δ_x	thickness of the intruding flow layers at the side walls, $(\kappa L/W_{\max})^{1/2}$
δ_z	thickness of the end wall thermal boundary layer, $(\kappa H/U_{\max})^{1/2}$
κ	thermal diffusivity
λ	distance of the maximum axial velocity to the nearest side wall
ν	cinematic viscosity
ρ	fluid density
Θ_x	dimensional temperature difference along the side walls at the core
ω	vorticity

Subscripts

I	value of the Rayleigh number at the thermal inversion
c	core flow solution

parameter K, defined as the ratio of the axial temperature gradient at the core region and the overall axial temperature gradient was one of the principal motivations and was used to distinguish between three unicellular flow regimes ordered in increasing Ra: the conductive regime ($K \approx 1$), the transition regime ($0 < K < 1$) and the boundary layer (or convective) regime ($K \approx 0$). The flow at large Ra has been another of the principal motivations of previous works concerning the horizontal case. The pioneer theoretical study of Gill [11] and the work of Patterson and Imberger [12] gave the basis for the understanding of this problem. In [12] it was shown by order of magnitude analysis that different scalings of the flow quantities were needed for the limits of $Pr < \mathrm{O}(1)$, $Pr \geqslant \mathrm{O}(1)$ and $A \sim \mathrm{O}(1)$, $A < \mathrm{O}(1)$. The low Pr range was studied by several authors [13–15]. In particular, in [15], numerical calculations for a wide range of Pr showed that for $1 \leqslant Pr \leqslant 100$ the flow quantities vary in less than about 10%, indicating that if convection of momentum is small (i.e., for $Pr \geqslant \mathrm{O}(1)$) the Prandtl number has a minor influence on the heat and mass rates. For fluids with $Pr \geqslant \mathrm{O}(1)$ at large Ra, Gill [11] and Patterson and Imberger [12] showed that the generation of vorticity and the heat discharge occur near the isothermal walls at thermal boundary layers of thickness $\delta_z \simeq Ra^{-1/4}H$. In the core the axial temperature gradient is vanishingly small ($K \simeq 0$) and, therefore, if the cavity is horizontally placed the buoyancy forces are absent. As a consequence, a stagnant region is formed at the center part of the layer and the flow at the core occurs only as a result of the entrainment of mass from the vertical boundary layers being confined in thin intruding flowing layers near the horizontal walls. Patterson and Imberger [12] were the first to claim that the heat and vorticity balances in the horizontal boundary layers for $Ra > A^{-12}$ (i.e., for squared cavities) should differ from those occurring if $Ra < A^{-12}$ (i.e., for long cavities). For long cavities ($A < 1$) the discharge of heat through a cross-section at the core deviates from the discharge at the isothermal wall due to conductive loss of heat outside the horizontal boundary layer. Patterson and Imberger studied the case $Pr \geqslant \mathrm{O}(1)$ and $A \sim \mathrm{O}(1)$ and their conclusions were confirmed later [16]. Recently, Boehrer [1] studied the case $Pr \geqslant \mathrm{O}(1)$ and $A < 1$. This author considered that in the horizontal boundary layers, the vorticity production of buoyancy is balanced by diffusion along the cross-stream direction and that the diffusive loss of heat is balanced by advection. Using this assumption, an estimation for the thickness of the horizontal boundary layers was obtained $(3.2(A^2Ra)^{-1/5}H)$ which fitted quite well with the previous experimental and numerical calculations.

Boehrer also obtained the frontiers of the flow regimes in long horizontal cavities at $A^2Ra \approx 10^2$ and $RaA^2 \approx 10^4$.

The investigation about the effect of inclined boundaries on the unicellular flow in cavities with end-to-end temperature difference is relatively much more scarce. Previous studies presented numerical calculations of the Nusselt number [2,5,6,17]. In some of these works [5,6,17], rather complicated multi-parametric empirical fits for the Nusselt number were proposed. A greater amount of work was devoted to a related problem: inclined cavities with $A > 1$. In these works, empirical fits for the Nusselt number were also proposed (see for instance [18,19]). Nevertheless, in the literature we have not found any results concerning the identification of the different flow regimes in the extended space of parameters (Ra, A, α).

This work investigates the unicellular flow regimes in cavities whose longest axis $(A < 1)$ is arbitrarily inclined and differentially heated between its ends. We consider $Pr \geqslant O(1)$ and long cavities $(A < 1)$ in the sense of Patterson and Imberger [12]. First, a solution for the parallel core flow is presented and discussed. Then the parameter K is calculated by means of an integral model similar to that proposed by Bejan and Tien [20]. Once K is calculated, the frontiers of the flow regimes are determined in the extended space of parameters (Ra, A, α). The last part of the study concerns the large Ra limit of the flow (the boundary layer regime). The flow near the end walls and the flow at the core are separately analyzed. An order of magnitude analysis is used to obtain an analytical expression for the Nusselt number in the boundary layer regime (BLR) in terms of Ra, A and α. The theoretical predictions have been validated by numerical calculations of the flow carried out for $Pr = 0.7$ and $Pr = 6.7$ and different aspect ratios. The prediction on the Nusselt number at large Ra has also been confirmed by the results reported by Wirtz and Tzeng [5,6].

2. Geometry and equations of motion

The geometry of the problem is shown in Fig. 1 for horizontal cavities, 1. It consists of a two-dimensional cavity with $A = H/L < 1$ filled with an incompressible fluid. The cavity is inclined at an angle α with respect to the gravity vector, $\boldsymbol{g} = g(\sin(\alpha)\hat{i} - \cos(\alpha)\hat{k})$. A temperature difference, ΔT, is maintained between the end walls and the side walls are adiabatic. Using the Boussinesq approximation and H, H^2/κ, κ/H and ΔT, respectively, as units of length, time, velocity and temperature, the dimensionless equations written in terms of the vorticity and the temperature are

$$\frac{1}{Pr}\left(\frac{\partial \omega}{\partial t} + \boldsymbol{v}\cdot\nabla\omega\right) = \nabla^2\omega + Ra\left(\frac{\partial T}{\partial z}\sin(\alpha) + \frac{\partial T}{\partial x}\cos(\alpha)\right), \tag{1}$$

$$\frac{\partial T}{\partial t} + \boldsymbol{v}\cdot\nabla T = \nabla^2 T, \tag{2}$$

where the vorticity is defined as

$$\omega = \frac{\partial u}{\partial z} - \frac{\partial w}{\partial x} \tag{3}$$

and the Rayleigh number and the Prandtl number are, respectively, defined as, $Ra \equiv g\beta\Delta T H^3/\nu\kappa$ and $Pr \equiv \nu/\kappa$. The walls are rigid and the no-slip condition is assumed. The thermal boundary conditions are

$$\frac{\partial T}{\partial x} = 0 \quad \text{at } x = 0, 1, \tag{4}$$

$$T(x, 0) = 0, \quad T(x, A^{-1}) = -1. \tag{5}$$

3. The parallel flow at the core

For $0° < \alpha < 90°$ the mechanical equilibrium is not possible and for any $\Delta T > 0$ a convective flow is established. The basic structure of the flow is similar to the flow in an horizontal cavity [21]. Two flow regions may be distinguished: the core region, containing a parallel clockwise flow and the end regions near the closing walls, where the parallel flow turns around. The velocity and temperature profiles of the parallel flow in the core region have the following form:

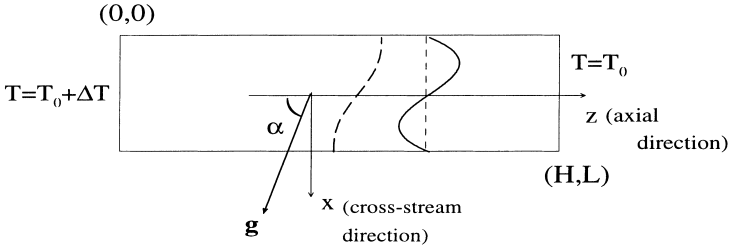

Fig. 1. Geometry of the problem.

$$\begin{aligned} &\boldsymbol{v}_c = w_c(x)\boldsymbol{k}, \\ &T_c(x,z) = -KAz + K\tau_c(x) + b, \end{aligned} \tag{6}$$

where b is a constant temperature and $-KA$ is the dimensionless temperature gradient in the core. A system of ordinary differential equations for $w_c(x)$ and $\tau_c(x)$ is obtained by substituting Eq. (6) into Eq. (2) and into the curl of Eq. (1). This system has three different types of solutions depending on the projection of the overall temperature gradient to the gravity vector

- Lateral heating: $\alpha = 90°$

$$w_c(x) = KARa\left(x^3/6 - x^2/4 + x/12\right), \tag{7}$$

$$\tau_c(x) = KA^2Ra\left(x^5/120 - x^4/48 + x^3/72\right). \tag{8}$$

- Heating from below: $0° < \alpha < 90°$

$$w_c(x) = \tan\alpha\left[\frac{2r(\sin r\sinh(r\hat{x}) - \sinh r\sin(r\hat{x}))}{\sinh r\cos r + \cosh r\sin r}\right], \tag{9}$$

$$\tau_c(x) = A\frac{\tan\alpha}{2}\left[\hat{x} - \frac{\sin r\sinh(r\hat{x}) + \sinh r\sin(r\hat{x})}{r(\sinh r\cos r + \cosh r\sin r)}\right]. \tag{10}$$

- Heating from above: $90° < \alpha < 180°$

$$w_c(x) = \tan\alpha\left[\frac{4r(\cosh r\sin r\sinh(r\hat{x})\cos(r\hat{x}) - \sin r\cos r\cosh(r\hat{x})\sin(r\hat{x}))}{\sinh r\cosh r + \sin r\cos r}\right], \tag{11}$$

$$\tau_c(x) = A\frac{\tan\alpha}{2}\left[\hat{x} - \frac{\sinh r\cos r\sinh(r\hat{x})\cos(r\hat{x}) + \cosh r\sin r\cosh(r\hat{x})\sin(r\hat{x})}{r(\sinh r\cosh r + \sin r\cos r)}\right]. \tag{12}$$

In Eqs. (9)–(12) we have used $\hat{x} \equiv 2x - 1$ and the parameter

$$\begin{aligned} &r \equiv \frac{1}{2}(KARa\cos\alpha)^{1/4} \quad \text{for } \alpha < 90°, \\ &r \equiv \frac{1}{2\sqrt{2}}(-KARa\cos\alpha)^{1/4} \quad \text{for } \alpha > 90°, \end{aligned} \tag{13}$$

where $KARa$ is the local Rayleigh number at the core region scaled with the axial temperature gradient at the core.

As seen in Eq. (1), the production of vorticity due to the x and z components of buoyancy are, respectively, proportional to $Ra\sin(\alpha)\partial T/\partial z$ and $Ra\cos(\alpha)\partial T/\partial x$. The temperature x-gradient is created by the flow advection and at low enough values of Ra it is negligibly small. Therefore, at small Ra and for any (not vertical) inclination the clockwise flow is generated by the x component of buoyancy. As Ra increases, a negative temperature x-gradient grows in the core by advection and generates vorticity owing to the z component of buoyancy. When heating from above ($\alpha > 90°$) the effect of the axial buoyancy is to suppress the clockwise convection in the center part of the layer, as long as $Ra\cos(\alpha)\partial T/\partial x < 0$ while $Ra\sin(\alpha)\partial T/\partial z > 0$. For large enough Ra and $\alpha > 90°$, the flow is confined to small regions near the walls where $\partial T/\partial x \approx 0$ as may be seen in Fig. 2. For $\alpha < 90°$, the production of vorticity of both components of buoyancy has the same sign and the

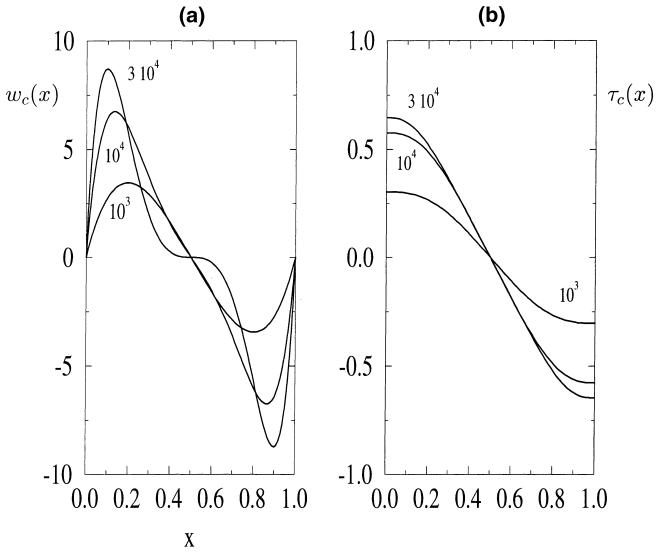

Fig. 2. Core flow profiles for $\alpha = 120°$. The numbers indicate values of the Rayleigh number at the core, $KARa$.

intensity of the flow increases with the cross-stream temperature gradient. In turn, the cross-stream temperature difference grows also with the flow intensity. Hence, for $\alpha < 90°$, the coupling of the velocity and temperature fields acts as a positive feedback that steeply enhances the flow convection as Ra increases. This kind of coupling leads to the divergence of the amplitude of the core flow solution (in Eqs. (9) and (10)) at a finite value of the local Rayleigh at the core: [1] $KARa = R_0\cos(\alpha)$, where $R_0 = 500.54$. This anomalous behavior of the core flow solution has been also reported in previous studies on natural convection with two components of the buoyancy force [7,22]. Flow properties as stability [22] or mass transport [7] were studied for values of $KARa$ below and above the divergence value. These works considered the limit of infinite cavities ($A \to 0$) and assumed that $KARa$ was a flow independent parameter. Although, for an infinite horizontal cavity the equality $K = 1$ holds [20,21], and therefore, $KARa$ may be considered to be flow independent, we shall show by considering the flow at the end walls of the cavity, that for $0° < \alpha < 90°$ the value of $KARa$ is bounded by $R_0/\cos(\alpha)$ for any arbitrarily small value of A. This means that the divergence of the core profiles is not to be observed and therefore the solutions Eqs. (9) and (10) have no physical meaning for $KARa > R_0/\cos(\alpha)$.

The value of R_0 is precisely the critical Rayleigh number for the onset of transversal perturbations in an infinite vertical cavity [22]. At $KARa\cos(\alpha) \to R_0$, the functional form of core profiles for $\alpha < 90°$ coincides with the critical transversal disturbance for the onset of convection in the vertical cavity [22]. This can be seen by considering the Laurent series of Eqs. (9) and (10) at $r = r_0$. In particular, for the axial velocity, one obtains

$$w_c(x) = \tan\alpha\left(\frac{2r_0\tan(r_0)}{(r-r_0)}\right)\left(\frac{\sinh(r_0x)}{\cosh(r_0)} + \frac{\sin(r_0x)}{\cos(r_0)}\right) + \mathrm{O}(r-r_0)^0. \tag{14}$$

4. Calculation of K

The parallel flow solution proposed for the core region in Eqs. (6)–(12) does not satisfy the boundary conditions at the end walls. These conditions must be satisfied by a solution for the end regions that match to the flow at the core. The parameters K and b are calculated using the matching conditions. Several methods are proposed in the literature [13,20,21]. We have used the method proposed by Bejan and Tien [20] which is a diffusive approximation and consequently gives results which are Pr-independent. Bejan and Tien's model assumes equal thickness for the momentum and temperature boundary layer at the end walls (which is certain for $Pr \sim \mathrm{O}(1)$), and as shown in previous works [1,15,20] it gives correct results for moderate to high Prandtl number.

The method consists of constructing a solution for the turning regions that matches up to first derivatives the flow at the core at a certain distance from the end walls, δ, that has to be also evaluated. The three equations needed to calculate K, b and δ come out from the centro-symmetry of the problem, $T(1/2, A^{-1}/2) = -1/2$, and from the two integral constraints obtained by integrating twice (from $x = 0$ to $x = 1$ and from $z = 0$ to $z = \delta$) the heat equation (2)) and the vorticity equation. Using these constraints one obtains, for any given value of α and A, the following relationships:

$$K(r) = \frac{1}{(1+F(r))}, \quad \text{with } F(r) \equiv \delta(r)\int_0^1 w_c(x)\tau_c(x)\,\mathrm{d}x, \tag{15}$$

where $F(r)$ is obtained from the core profiles in Eqs. (7)–(12) and $\delta = \delta(r)$ is obtained from the centro-symmetry condition and the integrated vorticity equation. Eq. (15) is, in fact, a system of transcendental equations (note that r depends on K) and has been solved by a Newton–Raphson method. Fig. 3(a) shows a plot of K versus Ra for $A = 0.1$. Circles correspond to values of K obtained from the numerical solution of the Navier–Stokes and heat equations (see Section 8) in the geometry indicated in Fig. 1. The agreement with the solution of Eq. (15), shown in Fig. 3(a) with solid lines, is excellent for $K > 0.1$ and the aspect ratios considered ($A < 0.25$).

Eq. (15) for K comes out from the balance of the heat advected from the core and diffused at the end region. Any increase in the amount of heat advected from the core increases the diffusion rate and consequently the temperature drops at the end region, therefore reducing the axial temperature gradient at the core, $K\Delta T/L$, with respect to the overall temperature gradient, $\Delta T/L$. For $Ra \to 0$, the advection term in Eq. (17) vanishes and $K \to 1$. The behavior of K at large Ra depends on the inclination angle. When heating from above, $\alpha > 90°$, the advection of heat decreases for Rayleigh number larger than a certain value and K reaches a minimum value as seen in Fig. 3(a). For $\alpha \leqslant 90°$, the amount of heat advected from the core increases monotonically with Ra and K tends to zero. At large enough Ra, when advection becomes dominant, we have observed that, in the horizontal cavity, K decreases approximately like

[1] Formally, the divergence of the core flow solution occurs for discrete values of r which satisfy $\tanh(r) + \tan(r) = 0$. The lowest value is $r = r_0 = 2.365$ and $R_0 = 2r_0^4$ (see Eq. (13)).

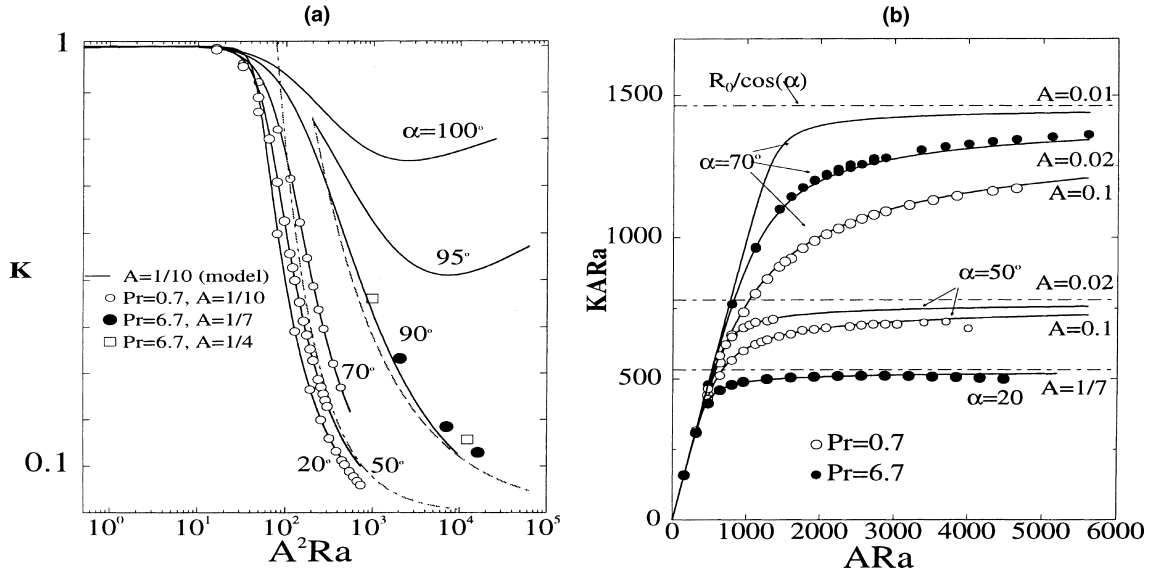

Fig. 3. (a) The parameter K against A^2Ra. The dashed line for $\alpha = 90°$ corresponds to the result of Boherer [1]: $K \sim (A^2Ra)^{-1/2}$. The dashed line for $\alpha = 50°$ corresponds to $K \sim (ARa\cos(\alpha)/R_0)^{-1}$. At (b) the local Rayleigh number at the core, $KARa$, versus ARa.

$10(A^2Ra)^{-1/2}$ in agreement with the result of Boehrer [1]. For $\alpha < 90°$ we have found the following trend for K:

$$K \to \frac{R_0}{ARa\cos(\alpha)} \quad \text{for } Ra \to \infty. \tag{16}$$

Eq. (16) implies that the local Rayleigh number at the core, $KARa$, tends asymptotically to $R_0/\cos\alpha$. This fact can be seen in Fig. 3(b), where the local Rayleigh number at the core $KARa$ is plotted versus ARa. Note that $KARa$ never reaches the limit value for the divergence of the parallel flow solution, $R_0/\cos\alpha$.

5. The frontier for the conductive regime

In the conductive regime (low Ra limit) the advection of heat is negligible and heat is transported by conduction so the isotherms are nearly parallel to the x-axis and $K \approx 1$. By introducing $K \approx 1$ into the relationship $K \simeq 10(RaA^2)^{-1/2}$, one obtains the frontier proposed by Boehrer [1] for the conductive regime, $RaA^2 \approx 10^2$. Bejan and Tien [20] found essentially the same frontier ($RaA^2 \approx 72$) by selecting a limiting value of the cross-stream temperature difference at the core: $\Theta_x < 0.1\Delta T$. Both criteria involve the group parameter RaA^2. In fact, as shown in [1], in horizontal cavities the group RaA^2, which measures the relative importance of horizontal (along z) advection compared to vertical (along x) conduction of heat, governs the type of flow regime. This is no longer valid in inclined cavities.

For $\alpha < 90°$, the type of flow regime is not controlled by the group A^2Ra but rather by $\mathscr{R} \equiv ARa\cos(\alpha)/R_0$. In particular, we have shown that in the transition regime the parameter K decreases with Ra like $K \simeq \mathscr{R}^{-1}$ so if $\alpha < 90°$, the conductive regime ($K \simeq 1$) exists for $\mathscr{R} \leqslant O(1)$. Considering that R_0 is the critical Rayleigh number for the onset of convection in a vertical infinite cavity, this result indicates that, in heated-from-below inclined cavities, the transition to an advection dominated flow takes place when the axial projection of buoyancy overpowers the thermal and viscous diffusion along the z-axis.

When heating from above ($\alpha > 90°$) the axial buoyancy acts as a restoring force that tends to suppress convection as long as cross-stream temperature differences are created. Hence, in this configuration it may occur, depending on α and A, that the flow remains in the conductive regime no matter how large the value of Ra is made. This fact is deduced from Fig. 3(a) which shows that for $\alpha > 90°$ the value of K reaches a minimum value. The calculation of K from Eq. (15) yields that for $\alpha > 90°$ the value of K satisfies

$$K \geqslant \frac{1}{1 + 0.190A\tan^2(\alpha)(\alpha - 90°)^{0.35}}. \tag{17}$$

Therefore, if for a particular configuration the minimum of K is approximately one, the flow shall remain in the conductive regime for any large value of Ra. As an example, Eq. (17) indicates that in a cavity with $A = 0.25$ and $\alpha > 120°$ the value of K shall be always greater than 0.9. Eq. (17) shows also a classic result of Cormack et al. [21]: in order to maintain the conductive regime at $Ra \to \infty$ in a horizontal cavity one has to choose it infinite, $A \to 0$.

6. The boundary layer regime

In this section, we consider the flow at the large Ra limit. At large Ra it may occur (if the value of α is low enough, as shown afterwards) that almost all the temperature drop is confined to small boundary layers near the end walls leaving very small temperature z-gradient at the core ($K \approx 0$). In the horizontal case, it has been also shown that intruding flow layers are developed along the $x = 0, 1$ walls. In order to determine the frontier of the BLR in the horizontal case, it is possible to use either a small limiting value of K or an argument involving the thickness of the intruding layer. For instance, Boehrer [1] calculated the frontier of the BLR by considering that the thickness of the intruding layer, $3.2(A^2Ra)^{-1/5}H$, should be smaller than $H/2$: this yields $RaA > 10^4$. Inserting this condition in the relationship $K \approx 10(RaA^2)^{-1/2}$, one obtains $K < 0.1$, which is precisely the requirement used in the previous work of Bejan and Tien [20] for the BLR presence. In inclined cavities the assumptions that lead to the core profiles in Eqs. (9) and (10) break down also for small enough values of K and, as shown below, the condition $K < 0.1$ is also representative of the processes involved at high Ra.

Prior to presenting our findings on the BLR for inclined cavities it is necessary to specify the region in which this type of regime can be observed. Eq. (17) indicates that the BLR can only take place in heated-from-below or nearly horizontal cavities. In particular, the range of inclinations in which the condition $K < 0.1$ is satisfied, varies from $\alpha \leqslant 90°$ in an infinite long cavity ($A \to 0$) to $\alpha < 93.5°$ in a nearly squared cavity of $A = 0.5$. Therefore, without much loss of generality we shall concern our study of the BLR of inclined cavities to the $\alpha < 90°$ case. In Fig. 4, the values of A^2Ra at which $K = 0.1$ are plotted versus α for several values of the aspect ratio. The circle placed at $\alpha = 90°$ and $A^2Ra \approx 10^4$ corresponds to the frontier for the BLR found by Boehrer [1]. As seen in Fig. 4, as $\alpha \to 90°$, our results recover the frontier for the horizontal case but, for $\alpha < 90°$, the frontier $K = 0.1$ is no longer determined by the group A^2Ra. Instead, considering that for $\alpha < 90°, K \simeq \mathscr{R}^{-1}$, the requirement $K < 0.1$ is approximately fulfilled for $\mathscr{R} > 10$. The dashed lines in Fig. 4 correspond to this approximation and fit well with the numerical results for $\alpha < 85°$.

6.1. Flow near the end walls

In the inclined case ($\alpha > 0$), the generation of x-flow near the boundaries occurs essentially in the same way as in the horizontal case. The maximum value of the x-velocity, $U_{\max}$, is located at the thermal boundary layers near the end walls and the x-flow is diffused towards the center of the cavity to a distant of order of the viscous

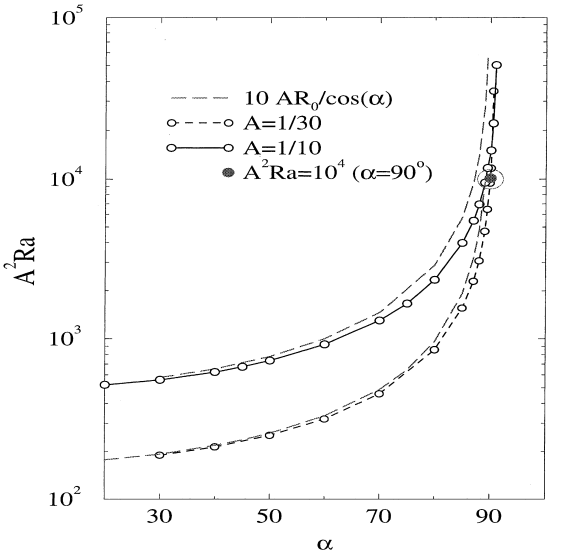

Fig. 4. The condition $K = 0.1$ in the A^2Ra–α space.

layer thickness, $O(Pr^{1/2}\delta_z)$. The thermal layer thickness can be derived from the balance of the advection along x and conduction along z-direction

$$\delta_z \simeq \left(\frac{\kappa H}{U_{\max}}\right)^{1/2}. \tag{18}$$

Let us estimate the magnitude of $U_{\max}$ for $0 \leqslant \alpha < 90°$. In an inclined cavity, $\alpha > 0$, the production of vorticity due to the x component of the buoyancy force at the thermal boundary layer $O(g\beta\Delta T \sin(\alpha)/\delta_z)$ is balanced by the viscous diffusion of vorticity $O(\nu U_{\max}/\delta_z^3)$. This balance gives $U_{\max} \sim Ra \sin(\alpha)(\delta_z/H)^2\kappa/H$. This reasoning is similar to the order of magnitude analysis made by Patterson and Imberger [12] for the horizontal case (see also [11]) and gives $U_{\max} \sim Ra^{1/2}$. In the case of a low aspect ratio vertical cavity ($\alpha = 0$) the onset of convection takes place at $Ra \simeq R_0$ and, for the Rayleigh number considered here ($Ra > 10A^{-1}R_0$) the end wall thermal boundary layers are yet developed. Hence, we propose the following relationship for $U_{\max}$ in the large Ra limit

$$U_{\max} = (c_0 + c_1 \sin(\alpha))^{1/2} Ra^{1/2}\kappa/H. \tag{19}$$

The thickness of the thermal boundary layer is by virtue of Eq. (18)

$$\delta_z/H = \left(c_0 + c_1 \sin^{1/2}(\alpha)\right)^{-1/2} Ra^{-1/4}, \tag{20}$$

where c_0 and c_1 are independent of Ra, α and A. Relationship (19) has been used to fit the numerically calculated values of $U_{\max}$ at several values of Ra, α and A for $Pr = 6.7$. This furnished: $c_0 = 0.105 \pm 0.005$ and $c_1 = 0.27 \pm 0.03$. In Fig. 5(a), the numerical results

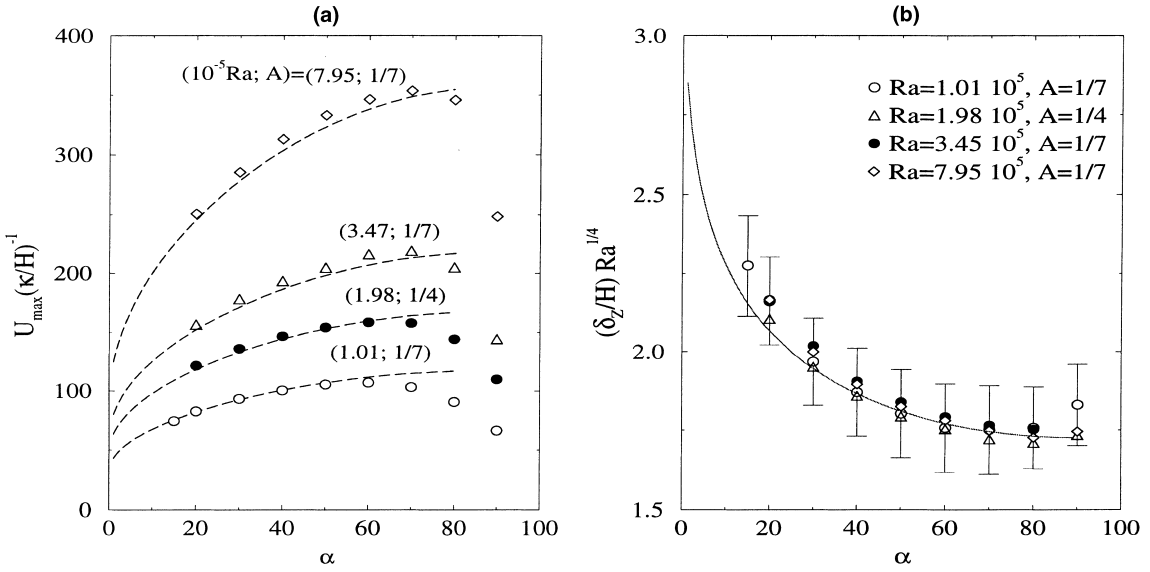

Fig. 5. (a) The maximum x-velocity $U_{\max}$, (b) scaled values of the end wall thermal boundary layer thickness $\delta_z Ra^{1/4}$. The dashed lines in (a) and (b) correspond, respectively, to Eqs. (19) and (20).

(circles) are compared with Eq. (19) (dashed lines). For cases lying in the range $\mathscr{R} > 10$, Eq. (19) correctly reproduces the numerical results but for those cases with $\mathscr{R} < 10$ (i.e., for large enough inclinations) the agreement is poor. Note that for $\mathscr{R} < 10$ the BLR is not yet developed and in the end regions the fluid flows by continuity. Hence in these cases, the magnitude of $U_{\max}$ and its dependence with α are similar to that observed for $W_{\max}$ (see Fig. 6(b)).

Relation (20) was verified by numerical calculations of δ_z carried out by recording the maximum value of the temperature diffusion across z-direction. The variation of δ_z along x-direction is about 10% and is indicated with error bars in Fig. 5(b). In Fig. 5(b) numerically

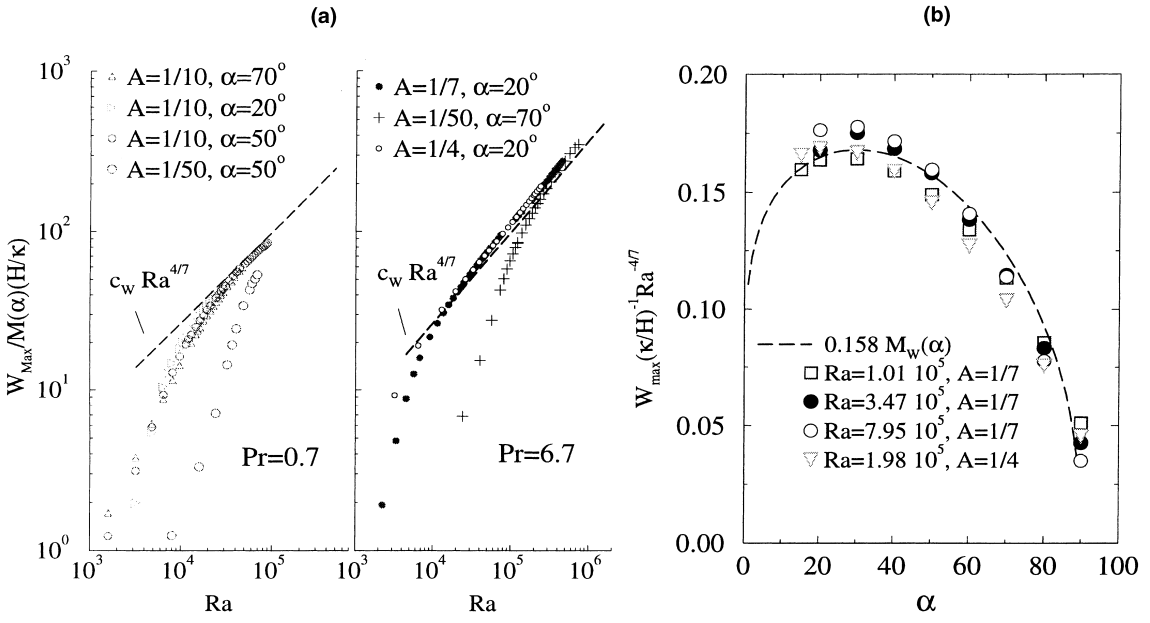

Fig. 6. (a) Values of $W_{\max}$ scaled with $1/M_w(\alpha)$ for different set of parameters and (b) $W_{\max}$, scaled with $Ra^{-4/7}$ versus α for data obtained with $Pr = 6.7$. The dashed lines correspond to the theoretical prediction of Eq. (23).

calculated values of δ_z and scaled with $Ra^{1/4}$ are plotted versus α for cases corresponding to $A = 1/7$, $A = 1/4$ and $Pr = 6.7$. The solid line in Fig. 5(b) corresponds to Eq. (20) (using the values of c_0 and c_1 obtained in the fit for $U_{\max}$). The excellent agreement found with the numerical results indicates that the order of magnitude analysis made for δ_z and $U_{\max}$ is correct.

Unfortunately, no representative results could be taken in the small-angle-range of the BLR because at the Rayleigh number considered the unicellular regime breaks down. At $Ra = 3.47 \times 10^5$, $15° \leqslant \alpha < 20°$; $Ra = 10^5, 12° \leqslant \alpha < 15°$ and $Ra = 1.98 \times 10^5, 10° \leqslant \alpha < 15°$ two oscillating Bernard-type counterclockwise cells appear at regions of order H near the ends of the cavity as a consequence of the large temperature z-gradient at the boundary layers.

6.2. Flow at the core region

We recall that in the BLR of horizontal cavities a diffusionless stagnant region develops in the center of the layer, a consequence of a vanishing buoyancy force at the core. In inclined cavities a completely different scenario takes place. Even if $K \approx 0$, buoyant production of vorticity exists in the core of the inclined cavity owing to the presence of cross-stream temperature difference and the z component of gravity. For $Pr \geqslant 1$ and $A < 1$, the convection of vorticity in the core is negligible compared to the diffusion and in this region Eq. (1) takes the following form:

$$\frac{\partial^3 w}{\partial x^3} \simeq -Ra\cos(\alpha)\frac{\partial T}{\partial x}. \tag{21}$$

Thus, if the cavity is inclined, the vorticity produced by buoyancy is diffused along x-direction and the stagnant, diffusionless core is not developed. For $K \approx 0$ the theoretical model yields an integrated version of the production–diffusion balance expressed in Eq. (21). Therefore, we considered it reasonable to study the $Ra \to \infty$ limit of the theoretical model to obtain an analytical expression for the magnitude of axial velocity at the core, $W_{\max}$. For $Ra \to \infty$ (i.e., for $r \to r_0$) the dominant term in the Laurent expansion of the velocity profile around $r = r_0$ (Eq. (14)) is proportional to $(r_0 - r)^{-1}$. Also, for $r \to r_0$ we have found the following behavior of the function $F(r)$:

$$F(r) = 0.680A\tan^2(\alpha)\frac{\cos^{2/5}(\alpha)}{\alpha^{1/2}}(r_0 - r)^{-7/4} + \mathrm{O}(r_0 - r)^{-3/2}. \tag{22}$$

At large $Ra, F(r) \gg 1$ and by virtue of Eq. (15), $K(r) = 1/F(r)$. Also, for $\mathscr{R} > 10, K = \mathscr{R}^{-1} + \mathrm{O}(\mathscr{R}^{-2})$. Neglecting the small contribution $\mathrm{O}(\mathscr{R}^{-2})$, both equalities yield: $K = 1/F = 1/\mathscr{R}^{-1}$. Using Eq. (22) one obtains an expression for $(r_0 - r)^{-1}$ in terms of Ra which can be introduced in the maximum value of the profile (14) to obtain the following prediction for the maximum axial velocity at the core:

$$W_{\max} = c_w Ra^{4/7} M_w(\alpha)\kappa/H \tag{23}$$

with the constant $c_w = 0.138$ and

$$M_w(\alpha) = \left(\frac{\alpha^{1/2}\cos^{3/5}(\alpha)}{0.680\tan^{1/4}(\alpha)}\right)^{4/7}. \tag{24}$$

Numerous calculations were carried out in the range $\mathscr{R} > 10$ in order to validate the relationship (23). Fig. 6(a) shows the numerically obtained values of $W_{\max}$ scaled with $1/M_w(\alpha)$ versus Ra. Data for different set of parameters A and α and Pr are included. No information about the Pr dependence is obtained from Eq. (23) so numerical data corresponding to $Pr = 0.7$ and $Pr = 6.7$ are presented in Fig. 6(a) in different plots to take into account this dependence. The dashed lines correspond to Eq. (23). The numerical results confirm surprisingly well the theoretical prediction for $W_{\max}$. Respectively for $Pr = 0.7$ and $Pr = 6.7$, the data for different values of α and A align to $0.129Ra^{4/7}\kappa/H$ and $0.158Ra^{4/7}\kappa/H$ and the theoretical prediction $(0.138Ra^{4/7}\kappa/H)$ coherently lies between both trends (we recall that the model assumes $Pr \simeq 1$). Fig. 6(b) shows values of $W_{\max}Ra^{-4/7}$ versus α for $Pr = 6.7$ and different values of Ra and A. The numerical results also agree quite well with the theoretical modulation $M_w(\alpha)$ expressed in Eq. (24). For $\mathscr{R} > 10$, the largest velocities at the core correspond to $\alpha \approx 30°$. This result coincides with previous studies on this type of configuration [2,5,6].

In order to get some insight on the shape of the core profiles in the BLR of inclined cavities, let us consider now the evolution of the temperature field with Ra in the range $\mathscr{R} > 10$. Fig. 7 shows pictures of isotherms at different stages of the flow for $\alpha < 90°$ and $\mathscr{R} > 10$. For $\mathscr{R}$ just above 10 (Fig. 7(a)) the isothermals become parallel to the z-axis at the center of the cavity and so in this region there is practically no diffusion of heat. If the cavity was horizontally placed, this situation would coincide with the formation of a stagnant core (i.e., advection would also be absent) and therefore the diffusionless temperature profile ($\partial T/\partial x = cte.$) would remain valid at higher values Ra [16,23]. This result does not apply in an inclined cavity. At the diffusionless region of the inclined cavity a balance is established between the advection of heat along x- and z-directions in such way that, as Ra increases, the isotherms tilt beyond the z-direction. At this stage (illustrated in Fig. 7(b)), $\partial T/\partial z$ changes its sign along the x-direction being positive in the center of the layer and negative near the $x = 0, 1$ walls. Consequently, the advection along z-direction tends to suppress the cross-stream temperature difference at the center of the layer while continues to

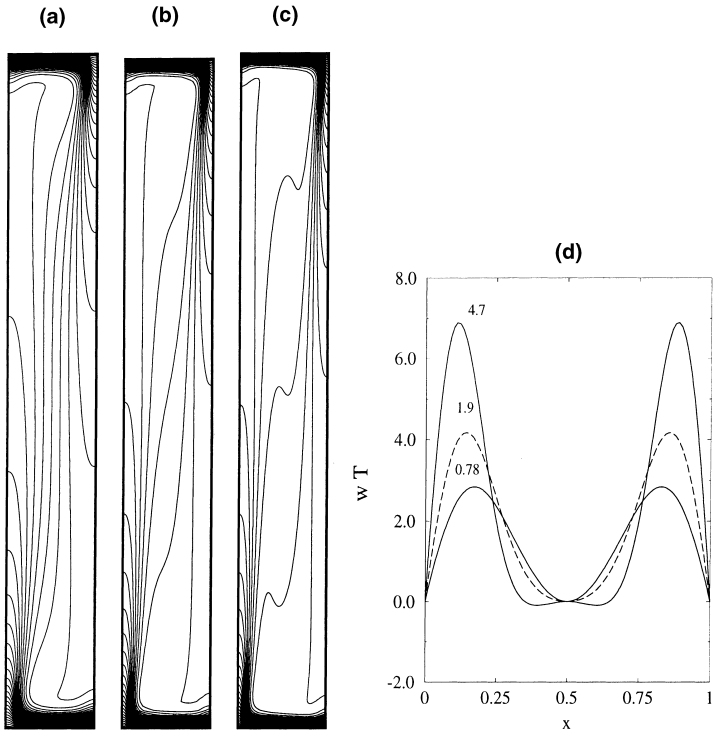

Fig. 7. Isothermals for $Pr = 6.7, A = 1/7$, $\alpha = 20°$ and (a) $Ra = 6.72 \times 10^4$; (b) 1.01×10^5 and (c) $Ra = 3.47 \times 10^5$. In (d) the product wT evaluated at the center of the cavity, $z = A^{-1}/2$. The values of $Ra \times 10^{-5}$ are indicated.

increase the temperature jump near the lateral walls at $x = 0, 1$. As a result, the largest temperature x-gradient in the core is concentrated in two boundary layers near the lateral walls where most part of the heat is transported along the core. This can be seen in Fig. 7(d) where the product wT is plotted against x for increasing Ra. The temperature x-gradient continues to decrease in the center of the layer and finally for $Ra > Ra_I$, a thermal inversion occurs (i.e., $\partial T/\partial x > 0$ around $x = 1/2$) as may be seen in Figs. 7(c) and 8(a). In the numerical calculations we observed that the change of sign of $\partial T/\partial x$ occurred at a fixed value of the group $\mathscr{R}$, which is independent on α. Respectively for $A = 1/7$ and $A = 1/4$ it was found, $\mathscr{R}_I = 75 \pm 1$ and 60 ± 1.

The cross-stream temperature difference at the core, Θ_x, is a particularly important flow quantity in inclined cavities because it determines the intensity of buoyant production (see Eq. (21)). It may also be used to estimate the Nusselt number, as we shall see below. The dependence of Θ_x with Ra may be seen in Fig. 9. As occurs in the horizontal case [16,23], as Ra increases, the value of Θ_x converges to an Ra-independent value that shall be noted with $\Theta_{x,f}$. We recorded the value of Ra at which Θ_x varied in less than about 1% and found that for any inclination the asymptotic value of Θ_x is reached at a fixed value of the group $\mathscr{R} = ARa\cos(\alpha)/R_0$ (in particular, $\mathscr{R} = 33 \pm 1$ and 27 ± 1, respectively, for $A = 1/7$ and $A = 1/4$ and $Pr = 6.7$). On the other hand, the numerical results indicate that the asymptotic value, $\Theta_{x,f}$, scales with $A^{4/7}$. Evidence is shown in Fig. 9 where the values of $\Theta_{x,f}A^{-4/7}$ are plotted against α. In conclusion, the calculated values of $\Theta_{x,f}$ fit within about 5% of error to

$$\Theta_{x,f} = M_T(\alpha)A^{4/7}\Delta T, \quad \text{where } M_T(\alpha) = 1.06 - 0.72\cos^{2/7}(\alpha). \tag{25}$$

Attention has also been given to the position of the maximum axial velocity because, apart from being an important feature of the shape of the velocity profile, it has been proved in previous works for horizontal configurations [1,23] that it provides a different means of monitoring the transition to the BLR. Let λ be the distance from the maximum (minimum) of the axial velocity in the core to the side wall at $x = 0$ ($x = 1$). The value of λ may be estimated from an order of magnitude analysis on the balance between diffusion and production of vorticity in the core in Eq. (21). Owing to the symmetry of the problem we shall consider only the maximum near $x = 0$. Around $x = \lambda/H$, the diffusion of vorticity is (in dimensionless units)

$$\frac{\partial^3 w}{\partial x^3} \simeq \frac{W_{\max}}{\lambda^3}\frac{H^4}{\kappa}. \tag{26}$$

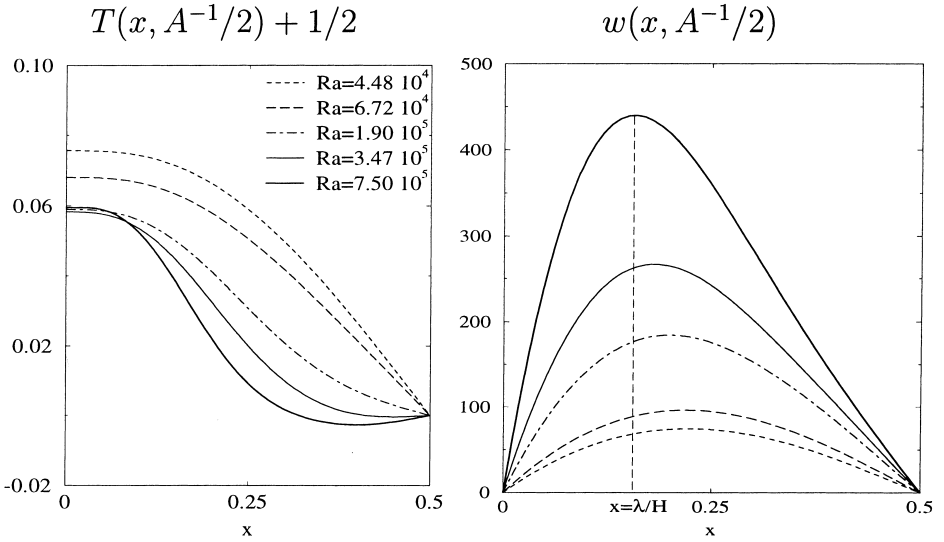

Fig. 8. Temperature and w-velocity x-profiles at the center of the cavity, $z = (2A)^{-1}$, for $A = 1/7, Pr = 6.7, \alpha = 20°$ and several values of Ra.

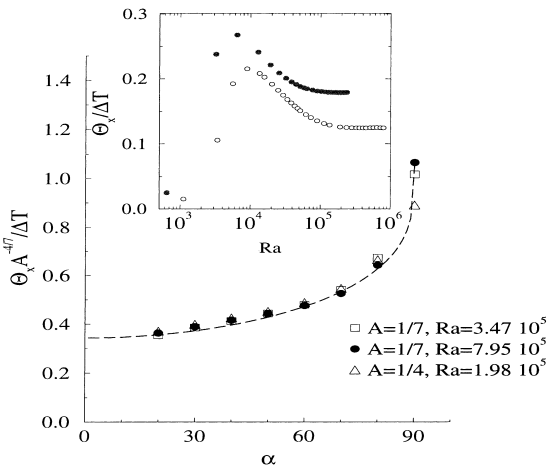

Fig. 9. $\Theta_x A^{4/7}$ versus α for several values of Ra, A and $Pr = 6.7$. In the upper part of the figure, Θ_x versus Ra for $Pr = 6.7, \alpha = 20°$ and $A = 1/7$ (open circles), $A = 1/4$ (filled circles).

By virtue of Eq. (21) the production of vorticity around $x = \lambda/H$ has to be evaluated by considering the cross-stream temperature gradient. An inspection of the temperature x profiles in Fig. 8(a) indicates that the estimation of $\partial T/\partial x$ has to be adapted to the transformations of the temperature field mentioned above. For $Ra < Ra_I$ ($Ra < 3.47 \times 10^5$ in Fig. 8) and for $Ra > Ra_I$ we propose the following estimations for the temperature x-gradient

$$\frac{\partial T}{\partial x} \simeq \frac{\Theta_x}{\Delta T} \quad \text{for } Ra < Ra_I, \tag{27}$$

$$\frac{\partial T}{\partial x} \simeq \frac{\Theta_x}{2\lambda}\frac{H}{\Delta T} \quad \text{for } Ra > Ra_I. \tag{28}$$

Note (see Fig. 8) that the estimation for $Ra > Ra_I$ of Eq. (28) takes into account that the temperature drop along x is concentrated near the lateral walls, where the axial advection is maxima. Introducing Eqs. (26) and (27) or (28) into Eq. (21) and using Eq. (23), one obtains the following trends for λ:

$$\lambda/H \simeq Ra^{-1/7}\left(\frac{c_w M_w(\alpha)}{\cos(\alpha)(\Theta_x/\Delta T)}\right)^{1/3} \quad \text{for } Ra < Ra_I, \tag{29}$$

$$\lambda/H \simeq Ra^{-3/14}\left(\frac{2c_w M_w(\alpha)}{\cos(\alpha)(\Theta_x/\Delta T)}\right)^{1/2} \quad \text{for } Ra > Ra_I. \tag{30}$$

Numerically calculated values of λ for $Pr = 6.7$ and $\alpha = 20°$ and two different aspect ratios, $A = 1/7$ and $A = 1/4$, are presented in Fig. 10 against the Rayleigh number. The arrows indicate the values of $\mathscr{R}$ at $\Theta_x = \Theta_{x,f}$ (within 1%) and at the occurrence of the thermal inversion, $\mathscr{R} = \mathscr{R}_I$. At the onset of the BLR ($\mathscr{R} \simeq 10$) the position of the maximum axial velocity profile begins to shift towards the lateral walls from its value at the conductive and transition regime ($\lambda = 0.225$). Once Θ_x has reached an Ra-independent value, it is observed a power-law decay of $\lambda \sim Ra^{-1/7}$ as predicted in Eq. (29). Then, for $Ra > Ra_I$ the slope of the calculated values of λ changes to $Ra^{-3/14}$, as indicates Eq. (30). The α dependence of λ has been observed by

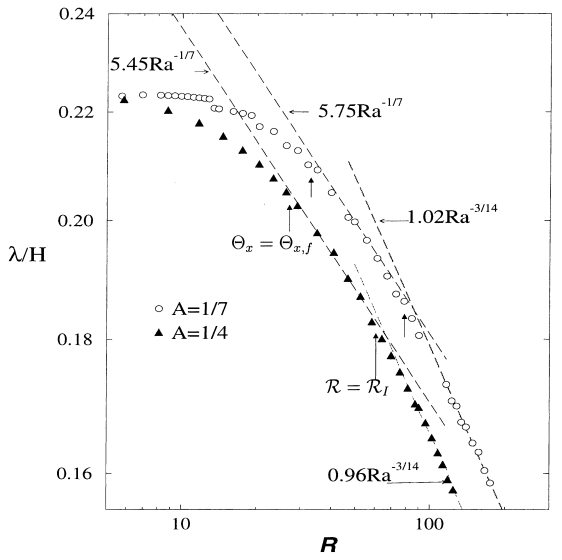

Fig. 10. Values of λ obtained for $\alpha = 20°$ and $Pr = 6.7$. Dashed lines correspond to the predicted trends in Eqs. (29) and (30) and arrows to the convergence of Θ_x and the occurrence of thermal inversion (see text).

scaling the calculated values of λ with $Ra^{1/7}$ and $Ra^{3/14}$. The results are shown in Fig. 11. In this figure, the number placed near each point is the value of the group $\mathscr{R}$. According to our predictions, for $A = 1/7$ points inside the range $33 < \mathscr{R} < \mathscr{R}_I = 75$ and $\mathscr{R} > 75$ should, respectively, coincide with the dependencies in Eqs. (29) and (30). The theoretical trends are drawn in solid lines in Fig. 11 and evidence the quantitative agreement with the numerically obtained values of λ.

7. The Nusselt number

The transport of heat along the axis of the cavity, represented by the Nusselt number, *Nu*, is not only an useful quantity in the application field but also a parameter that characterizes the type of flow regime. The Nusselt number is defined as the ratio between the heat transfer rate per unit width carried along z-direction and the heat that would be transferred by conduction in absence of flow due to the imposed end wall temperature difference. For adiabatic side walls *Nu* is independent on the z coordinate

$$Nu = \int_0^1 \left(\frac{\partial T}{\partial z} - wT \right) \mathrm{d}x \text{ at constant } z. \tag{31}$$

The calculation of *Nu* in slender inclined cavities with axial heating was carried out in some previous works [5,6,2,24]. In [24] we reported calculations of *Nu* for *Ra* below the boundary layer limit ($\mathscr{R} < 10$). In this section we shall concentrate our attention in the behavior of *Nu* at the large *Ra* limit of inclined $\alpha < 90°$ cavities. For $\mathscr{R} > 10$ the axial temperature gradient in the core vanishes and the product $w(x,z)T(x,z)$ only differs from zero in the boundary layers close to the walls at $x = 0, 1$ (see Fig. 7(d)). Therefore, the Nusselt number may be

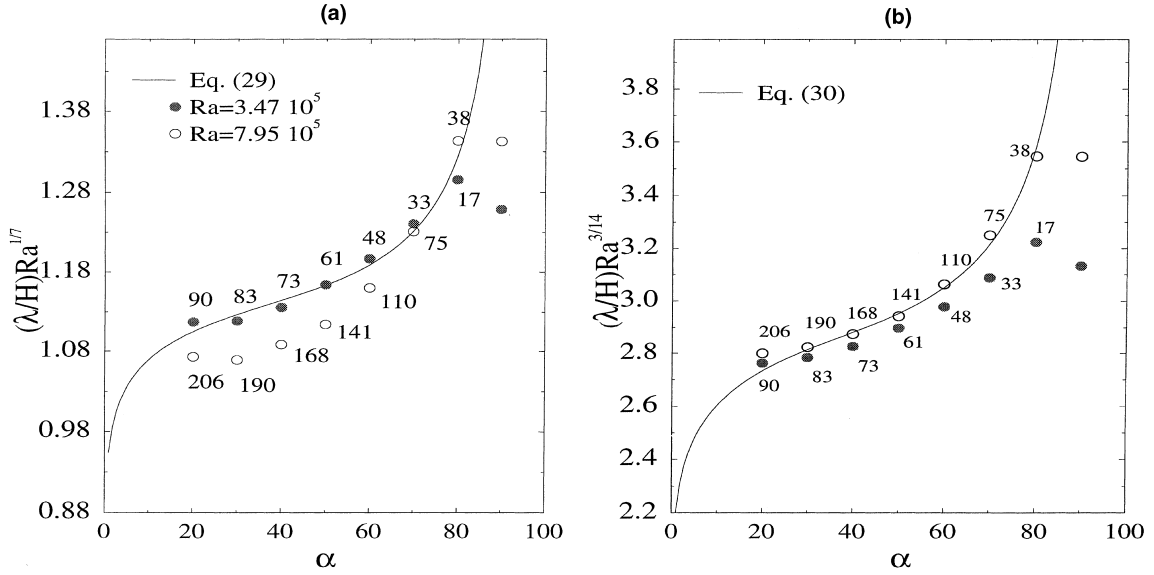

Fig. 11. Scaled values of λ versus α for $Pr = 6.7$ and $A = 1/7$. The numbers beside each point are the values of $\mathscr{R}$. The solid lines in (a) and (b) are fits to the numerical data using, respectively, the α dependence of Eqs. (29) and (30). The constants for the fits are 0.71 for Eq. (29) and 0.99 for Eq. (30).

estimated using a sort of mean value theorem for the integral of the product wT

$$Nu \simeq W_{\max}\Theta_x\delta_x/(\kappa\Delta T), \tag{32}$$

where δ_x is the thickness of the boundary layers where heat is transported by the axial flow. As argued by Patterson and Imberger [12], as the flow crosses the core of long cavities (i.e., for $Ra < A^{-12}$) some heat is lost by conduction outside the lateral boundary layers. Under this situation (see [1]), the thickness δ_x has to be estimated by considering the balance of heat advected along z-direction $O(W_{\max}\Delta T/L)$ with the heat diffused in the x-direction $O(\kappa\Delta T/\delta_x)$. This yields

$$\delta_x \simeq (\kappa L/W_{\max})^{1/2}. \tag{33}$$

Introducing Eq. (33) into Eq. (32) and using the expression for $W_{\max}$ (Eq. (23)) and for $\Theta_{x,f}$ (Eq. (25)), one obtains the following relationship for Nu, which should be valid for $\mathscr{R} > 10$

$$Nu \simeq c_w^{1/2}M_w^{1/2}(\alpha)M_T(\alpha)Ra^{2/7}A^{1/14}, \tag{34}$$

where $c_w = 0.138$ for the model's prediction of Eq. (23) while for $Pr = 6.7$ and $Pr = 0.7$ the fitted values are, respectively, 0.158 and 0.129. In order to compare results from different set of parameters let us define the *reduced* Nusselt number, $Nu_{\mathscr{R}}$

$$Nu_{\mathscr{R}} \equiv Nu\left(M_w^{-1/2}(\alpha)M_T^{-1}(\alpha)A^{2/7}\cos^{2/7}(\alpha)\right) \tag{35}$$

and rewrite Eq. (34) in terms of the group parameter $\mathscr{R}$

$$Nu_{\mathscr{R}} \simeq c_w^{1/2}R_0^{2/7}\mathscr{R}^{2/7}A^{1/14}. \tag{36}$$

The prediction for the Nusselt number has been tested using our numerical calculations and those captured from the papers of Wirtz and Tzeng [5,6]. Fig. 12(a) shows values of Nu scaled with $Ra^{-2/7}$ versus the inclination angle. The solid line corresponds to the theoretical trend in Eq. (34). Qualitative and also quantitative agreements are quite good. As shown in previous works [2,5,6,17,24], for $\mathscr{R} < 10$ the angle of maximum heat transfer increases with Ra inside the range $55° \leqslant \alpha \leqslant 65°$. As $\mathscr{R}$ increases above 10, the angle for maximum heat transfer shifts progressively towards $\alpha \simeq 80°$. This was observed in [5,6,17] and it is also seen in the $A = 1/7$ data of Fig. 12(a). Eq. (34) predicts a maximum heat transfer at $\alpha = 79°$.

Fig. 12(b) shows the reduced Nusselt number $Nu_{\mathscr{R}}$ (Eq. (35)) versus $\mathscr{R}$ for several sets of parameters with $Pr = 6.7$. Results from the works of Wirtz and Tzeng [5,6] corresponding to $A = 1/2, \alpha = 70°$ and $Pr = 6.8$ are also included. The data align clearly to the predicted 2/7 power-law which is indicated in dashed lines. We have included the prediction of Eq. (36) to explicit the quantitative agreement. With respect to the dependence

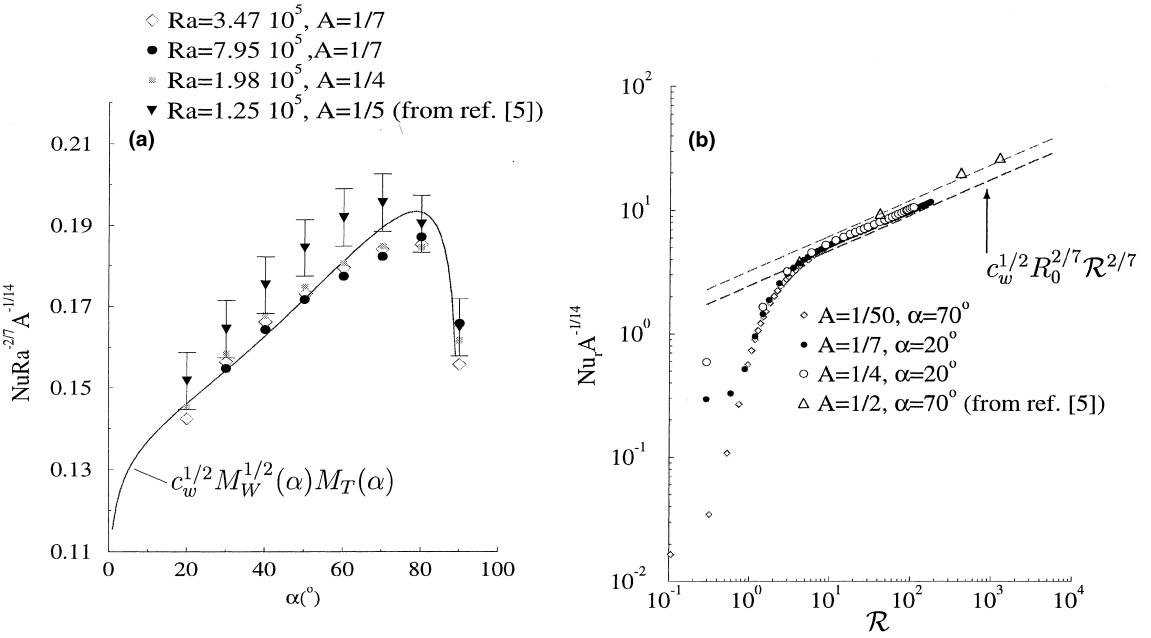

Fig. 12. (a) Nusselt number scaled with $Ra^{-2/7}A^{-1/14}$ versus α for different set of parameters. The symbols correspond to numerical calculations carried out in this work for $Pr = 6.7$ and also extracted from [5,6] (for $Pr = 6.8$). The solid line is the α dependence obtained from Eq. (34); (b) the reduced Nusselt number, Nu_r defined in Eq. (35), scaled with $A^{-1/14}$ and plotted versus $\mathscr{R}$. In the graph, the lowest dashed line is the theoretical trend in Eq. (36) and the upper one uses the same trend to fit the data obtained from [5,6].

of Nu with A, we have found that the calculated values of $Nu_{\mathscr{R}}\mathscr{R}^{-2/7}$ increase about 20% for $1/50 \leqslant A \leqslant 1/4$ and $\mathscr{R} > 10$. When introducing the $A^{1/14}$ dependence predicted in Eq. (36) this variation (always increasing with A) is reduced to less than 7%. Nevertheless, it is likely to occur that the A dependence of Nu for large Pr does not exactly fit to a power-law. In the case of horizontal cavities for $Pr > \mathrm{O}(1)$ and large (finite) Ra, an increase of about 20% in the value of Nu was found in [15] for $0.1 \leqslant A \leqslant 0.025$ and $Ra = 6 \times 10^6$. This increment was attributed to the increasing enclosure flow resistance and, as reported in [15], could not be fitted to a power-law dependence. This is consistent with our observations in inclined cavities.

8. Numerical solution of the flow

A Chebyshev-collocation pseudo-spectral method was used to solve the Navier–Stokes and heat equations in vorticity-stream function variables in the closed geometry of Fig. 1. The spatial approximation in both directions was done by expanding the flow variables in truncated series of Chebyshev polynomials [25]. The time integration was obtained through an Adam–Bashforth, second-order Backward Euler scheme. The diffusive terms are treated implicitly while the non-linear terms are treated explicitly. For each time cycle, the equation for the temperature at the next time step consists of a Helmholtz-type equation which is solved by means of a double diagonalization procedure for the algebraic system that arises in the Chebyshev-collocation method [25]. The equations relating the stream function and vorticity consist of a Stokes-type problem which is solved by the influence matrix technique [25]. This technique avoids the inconvenience of having two boundary conditions for the stream function and none for the vorticity and leads to the solution of several Helmholtz equations with Dirichlet boundary conditions. In most part of the calculations, the external Rayleigh number was gradually increased and the initial condition was the converged solution for the immediately lower Ra. In order to study the effect of the inclination angle, in some cases the Rayleigh number was fixed at a constant value while the inclination angle was gradually varied. The number of collocation points used in the calculations was varied to ensure accuracies of less or about 1%. The size of the meshes varied from 31×61 for the lowest aspect ratios and Rayleigh number considered ($A = 1/4$) to 35×256 for the longest cavities ($A = 1/50$). Typical sizes of the time step were about $10^{-4}H^2/\nu$ for the conductive regime and $10^{-5}H^2/\nu$ for the BLR. In order to arrive at the steady state, we have to wait transitories of about L^2/ν in the conductive regime which decreased like $L/W_{\max}$ in the BLR (for instance, $0.05L^2/\nu$ for $Ra = 4 \times 10^3$).

9. Conclusions

We investigated the unicellular flow in cavities whose longest side is arbitrarily inclined and supports a temperature difference between its ends. The conclusions of this work may be applied to cavities with $A < 1$ and $Pr \geqslant \mathrm{O}(1)$. In particular we have verified them by numerical calculations done for $0.02 \leqslant A \leqslant 0.25$ and $Pr = 0.7,\ 6.7$. The dimensionless axial temperature gradient at the core (K) was used to delimit the frontier of the three flow regimes: the conductive regime ($K \approx 1$), the transition regime ($0 < K < 1$) and the boundary layer regime ($K \approx 0$). If the cavity is not horizontally placed ($\alpha \neq 90°$) two completely different situations arise depending on the inclination angle. For $90° < \alpha < 180°$ (fluid heated from above) the axial component of buoyancy tends to suppress the convection as Ra increases and the parameter K reaches a minimum value at a certain Ra. Thus it may occur, depending on α and A, that the flow remains in the conductive or the transition regime for arbitrary large Ra. As an example, for $A = 0.25$ the conductive regime should always hold for $\alpha > 120°$ and the BLR is not to be observed if $\alpha > 93°$. For $0° < \alpha < 90°$ (fluid heated from below) the axial buoyancy amplifies the convection and K tends to vanish as Ra increases. We have found that in this configuration the governing parameter is $\mathscr{R} \equiv ARa\cos(\alpha)/R_0$ instead of A^2Ra which governs the type of flow in the horizontal case [1]. The parameter K decreases like $K \simeq \mathscr{R}^{-1}$ and the frontiers of the flow regimes are found at $\mathscr{R} \simeq 1$ and $\mathscr{R} \simeq 10$. The frontiers found by Boehrer for a long horizontal cavity $A^2Ra \simeq 10^2$ and $A^2Ra \simeq 10^4$ are recovered as α increases above approximately 85°. For smaller inclinations the flow at the core is controlled by the axial component of the buoyancy force.

In the investigation of the large Ra limit for heated-from-below inclined cavities, it has been shown that a careful order of magnitude analysis yields analytical relationships which are in qualitative and quantitative agreement with the numerical results. In the inclined case, the flow at the end wall boundary layers is governed by the same mechanism described for the horizontal case (see [11,12]). The maximum x velocities are proportional to $Ra^{1/2}$ and located at thermal boundary layers whose thickness is $\delta_z \sim Ra^{-1/4}$. The main differences with respect to the horizontal configuration are found in the core region owing to the existence of the axial component of buoyancy. We found that the maximum axial velocity at the core increases like $Ra^{4/7}$. This is faster than the proportionality observed for $\alpha = 90°$ (from [1], $Ra^{2/5}$). The shape of the core flow in the BLR is also greatly modified if the cavity is inclined. Although, as occurs for $\alpha = 90°$, the positions of the maximum and minimum of the axial velocity shift towards the side walls as Ra increases, if the

cavity is inclined, no stagnant core is formed in the center of the layer but rather a region of (approximately) constant shear. Also, as Ra increases the cross-stream temperature gradient does not reach an asymptotic constant value at the core as occurs for $\alpha = 90°$ (see [16,3]). Instead, it decreases and changes its sign at the center of the layer while continues to increase near the lateral walls at $x = \{0, 1\}$. This leads to the formation of two lateral boundary layers where most part of the cross-stream temperature jump and the heat transport along the core takes place. The lateral boundary layer thickness is determined by a conductive–advective balance of heat (see [1]). By estimating the rate at which heat is advected inside the lateral boundary layers, an analytical expression for the Nusselt number has been obtained. This relationship predicts $Nu \sim Ra^{2/7}$ and has been confirmed by our numerical calculations and those reported in previous works [5,6]. The $2/7$ exponent is also larger than those typically observed in the horizontal case ($\sim$1/5) [20,15]. Interesting enough is that the $2/7$ power-law is very close to the exponents found in the empirical fits to $Nu \sim Ra^n$ obtained in a related configuration: inclined cavities with $A > 1$. In [18] and [19], respectively, $n = 0.29$ and $n = 0.275$. Also in [18] it was mentioned that results for Nu at different angles could be fitted with the same exponent for Ra.

To conclude, it is important to mention how the results of this work may be altered by a third dimension in the cavity. As observed in previous works [26] for $Pr > O(1)$ and $\alpha < 90°$, thermal three-dimensional instabilities may develop if the third dimension of the cavity is typically more than $2H$, but these instabilities do not appear if it is made shorter. We have carried out calculations in three-dimensional cavities with nearly squared cross-section which shall be reported elsewhere. The flow is essentially two-dimensional in the core and the conclusions of the present work are applicable. An important conclusion is that if one calculates the value of R_0 in terms of the third dimension aspect ratio and uses it to redefine the parameter $\mathscr{R}$, the frontiers of the flow regimes are found at similar values of the rescaled group parameter: $\mathscr{R} \approx 1$ and 10.

Acknowledgements

We gratefully acknowledge P. Bontoux, M.A. Rubio, and I. Zuñiga. This work has been supported by DGICYT projects PB93-292 and PB94-382n and A. I. Hispano–Francesa 298B. Part of the numerical computations has been carried out on Cray YMP2E and CRAY C98 computers with support from IMT in Chateau-Gombert, Marseille.

References

[1] B. Boehrer, Convection in a long cavity with differentially heated end walls, Int. J. Heat Mass Transfer 40 (17) (1997) 4105–4114.
[2] B.L. Markham, F. Rosenberger, Diffusive-convective vapor transport across horizontal and inclined rectangular enclosures, J. Cryst. Growth 67 (1984) 241.
[3] P. Bontoux, C. Smutek, A. Randriamampianina, B. Roux, G.P. Extremet, A.C. Hurford, F. Rosemberger, De Vahl Davis, Numerical solutions and experimental results for three-dimensional buoyancy driven flows in tilted cylinders, Adv. Space Res, Pergamon, New York, 1986, p. 155.
[4] G.S.H. Lock, J. Fu, Natural convection in the inclined cranked thermosyphon, J. Heat Transfer 115 (1993) 167–172.
[5] R.A. Wirtz, W.F. Tsheng, Natural convection across tilted rectangular enclosures of small aspect ratio, in: J. Catton, K.E. Torrance (Eds.), Natural Convection in Enclosures, vol. 8, ASME, New York, 1980, pp. 54–67.
[6] R.A. Wirtz, W.F. Tsheng, Finite Difference simulation of free convection in tilted enclosures of low aspect ratio, in: Lewis, Morgan (Eds.), Numerical Methods in Thermal Problems I, Pineridge, Swansea, UK, 1979, pp. 381–390.
[7] A.W. Woods, S.J. Lintz, Natural convection and dispersion in a tilted fracture, J. Fluid Mech. 241 (1992) 59.
[8] P. Cessi, W.R. Young, Fixed-flux convection in a tilted slot, J. Fluid Mech. 237 (1992) 57.
[9] R. Delgado-Buscalioni, E. Crespo del Arco, Stability of thermally driven shear flows in long inclined cavities with end-to-end temperature difference, Int. J. Heat Mass Transfer 42 (1999) 2811–2822.
[10] P. Cerisier, S. Rahal, Experimental study of the competition between convective rolls in an enclosure, in: Annie Steinchen (Ed.), Dynamics of Multiphase Flows across Interfaces, Pergamon, Oxford, 1995, p. 105.
[11] A.E. Gill, The boundary layer regime for convection in a rectangular cavity, J. Fluid Mech. 26 (1966) 515–536.
[12] J. Patterson, J. Imberger, Unsteady natural convection in a rectangular cavity, J. Fluid Mech. 100 (1980) 65–86.
[13] J.E. Hart, Low Prandtl number convection between differentially heated end walls, Int. J. Heat Mass Transfer 26 (1983).
[14] J.E. Drummond, S.A. Korpela, Natural convection in a shallow cavity, J. Fluid Mech. 182 (1987) 543–564.
[15] G.S. Shiralkar, C.L. Tien, A numerical study of laminar natural convection in shallow cavities, J. Heat Transfer 103 (1981) 226–231.
[16] R.A.W.M. Henkens, C.J. Hoogendoorn, Scaling of the laminar natural-convection flow in a heated square cavity, Int. J. Heat Mass Transfer 36 (11) (1993) 2913–2925.
[17] J.C. Grondin, B. Roux, Search for simple relationships expressing the convective losses in a two-dimensional inclined cavity subjected to differential heating, Revue de Physique Appliquee 14 (1979) 49–56.
[18] J.N. Arnold, I. Catton, D.K. Edwards, Experimental investigation of natural convection in inclined rectangular regions of differing aspect ratios, J. Heat Transfer. Trans. ASME 68 (1976) 67–71.

[19] F.J. Hamady, J.R. Lloyd, H.Q. Yang, K.T. Yang, Study of natural convection heat transfer in an inclined enclosure, Int. J. Heat Mass Transfer 32 (9) (1989) 1697–1708.
[20] A. Bejan, C.L. Tien, Laminar natural convection heat transfer in a horizontal cavity with different end temperatures, J. Heat Transfer 100 (1978).
[21] D.E. Cormack, L.G. Leal, J. Imberger, Natural convection in a shallow cavity with differentially heated end walls, Part 1. Asymptotic Theory, J. Fluid Mech. 65 (1974) 209.
[22] G.Z. Gershuni, E.M. Zhukhovitskii, Convective stability of incompressible fluids, Israel Program for Scientific Translations, Jerusalem, 1976.
[23] P. Bontoux, B. Roux, G.H. Schiroky, B.L. Markham, F. Rosemberger, Convection in the vertical midplane of a horizontal cylinder. Comparison of two-dimensional approximations with three-dimensional results, Int. J. Heat Mass Transfer 29 (2) (1986) 227–240.
[24] R. Delgado-Buscalioni, E. Crespo del Arco, J. Ouazzani, P. Bontoux, Mean and secondary flow contribution to the heat transfer in an inclined slender box with axial heating, in: G. de Vahl Davis, E. Leonardi (Eds.), Advances in Computational Heat Transfer, Belgell House Inc., 1997, pp. 354–361.
[25] J.M. Vanel, R. Peyret, P. Bontoux, A pseudospectral solution of vorticity-stream function equations using the influence matrix technique, in: K.W. Morton, M.J. Baines (Eds.), Numerical Methods for Fluid Dynamics II, Clarendon Press, Oxford, 1986, pp. 463–475.
[26] R. Delgado-Buscalioni, E. Crespo del Arco, P. Bontoux, J. Ouazzani, Convection and instabilities inclined differentially heated rectangular boxes, Comptes Rendues Acad. Sci. Paris, t. 236, Série II, 1998, pp. 711–718.